

**Distribution of Faraday Rotation Measure
in Jets from Active Galactic Nuclei
II. Prediction from our Sweeping Magnetic Twist Model
for the Wiggled Parts of AGN Jets and Tails**

Hiromitsu Kigure^{1,2}, Yutaka Uchida^{2,3},
Masanori Nakamura^{2,4}, Shigenobu Hirose^{2,5}, and Robert Cameron^{2,6}

ABSTRACT

Distributions of Faraday rotation measure (FRM) and the projected magnetic field derived by a 3-dimensional simulation of MHD jets are investigated based on our "sweeping magnetic twist model". FRM and Stokes parameters were calculated to be compared with radio observations of large scale wiggled AGN jets on kpc scales. We propose that the FRM distribution can be used to discuss the 3-dimensional structure of magnetic field around jets and the validity of existing theoretical models, together with the projected magnetic field derived from Stokes parameters. In the previous paper, we investigated the basic straight part of AGN jets by using the result of a 2-dimensional axisymmetric simulation. The derived FRM distribution has a general tendency to have a gradient across the jet axis, which is due to the toroidal component of the magnetic field generated by the rotation of the accretion disk. In this paper, we consider the wiggled structure of the AGN jets by using the result of a 3-dimensional simulation. Our numerical results show that the distributions of FRM and the projected magnetic field have a clear correlation with the large scale structure of the jet itself, namely, 3-dimensional helix. Distributions, seeing the jet from a certain direction, show a good matching with those in a part of 3C449 jet. This suggests that the jet has a helical structure and that the magnetic field (especially the toroidal component) plays an important role in the dynamics of the wiggle formation because it is due to a current-driven helical kink instability in our model.

Subject headings: galaxies: jets — galaxies: magnetic fields — MHD — polarization

¹Kwasan and Hida Observatories, Kyoto University, Yamashina, Kyoto 607-8471, Japan; kigure@kwasan.kyoto-u.ac.jp

²Department of Physics, Science University of Tokyo, 1-3 Kagurazaka, Shinjuku-ku, Tokyo 162-8601, Japan

³Deceased, August 17, 2002.

⁴Jet Propulsion Laboratory, California Institute of Technology, 4800 Oak Grove Drive, Pasadena, CA 91109, USA

⁵Department of Physics and Astronomy, Johns Hopkins University, Baltimore, MD 21218-2686, USA

⁶Max-Planck-Institut für Aeronomie, Max-Planck-Straße 2, D-37191 Katlenburg-Lindau, Germany

1. Introduction

To explain the formation of active galactic nucleus (AGN) jets and other astrophysical jets, various models have been proposed. Among them, the magnetohydrodynamic (MHD) model is one of the most promising models, since it can explain both the acceleration and the collimation of the jets (see, e.g., Meier, Koide, & Uchida 2001, and references therein). Lovelace (1976) and Blandford (1976) first proposed the theoretical model of the magnetically driven jet from accretion disks, and Blandford & Payne (1982) discussed magneto-centrifugally driven outflow from a Keplerian disk in steady, axisymmetric and self-similar situation. Time-dependent, 2-dimensional axisymmetric simulations were performed by Uchida & Shibata (1985), Shibata & Uchida (1986), Uchida & Shibata (1986). They pointed out that large amplitude torsional Alfvén waves (TAWs) generated by the interaction between the accretion disk and a large scale magnetic field play an important role. The toroidal magnetic field propagates along the large scale magnetic field while squeezing it into a collimated jet-shape by the pinching effect of the Lorentz force. In this paper, we refer this model as a "sweeping magnetic twist model". After these papers, many authors have performed time-dependent, 2-dimensional axisymmetric simulations (e.g. Stone & Norman 1994, Ustyugova et al. 1995, Matsumoto et al. 1996, Ouyed & Pudritz 1997, Kudoh, Matsumoto, & Shibata 1998).

Using the numerical data of MHD models, observational quantities such as Faraday rotation measure (FRM) or Stokes parameters have been derived to be compared with observations of AGN jets: Laing (1981) computed the total intensity, the linear polarization, and the projected magnetic field distributions, assuming some simple magnetic field configurations and high energy particle distributions in the cylindrical jet. Clarke, Norman, & Burns (1989) performed 2-dimensional MHD simulations in which a supersonic jet with a dynamically passive helical magnetic field was computed, and derived distributions of the total intensity, the projected electric field, and the linear polarization. Hardee & Rosen (1999) calculated the total intensity and the projected magnetic field distributions, using 3-dimensional MHD simulations of strongly magnetized conical jets. Hardee & Rosen (2002) calculated the FRM distribution and discussed that the observation of the radio source 3C465 in Abell cluster A2634 (Eilek & Owen 2002) suggests helical twisting of the flow.

FRM is given by the integral of $n_e B_{\parallel}$ along the line-of-sight between the emitter and the observer (where B_{\parallel} is the line-of-sight component of the magnetic field, and n_e is the electron density there). It is, in principle, not possible to specify which part on the line-of-sight the contribution comes from. However, in recent high-resolution radio observations (e.g. Eilek & Owen 2002, Asada et al. 2002), the FRM distribution seems to have good correlation with the configuration of the jet; this suggests that the FRM variation is due to the magnetized thermal plasma surrounding the emitting part of the jet. In fact, sharp FRM gradients seen in 3C273 can not be produced by a foreground Faraday screen (Taylor 1998, Asada et al. 2002). If this is the case, we can get a new information, that is, the line-of-sight component of the magnetic field, and thus can predict the 3-dimensional configuration of the magnetic field around the jet, together with the projected magnetic field.

Uchida et al. (2004) (hereafter paper I) carried out a 2-dimensional axisymmetric simulation, and investigated the model counterpart distributions of FRM and the projected magnetic field in the basic straight part of AGN jets. It was described how a systematically helical field configuration is produced in the "sweeping magnetic twist model". It was also shown as a result that the model can reproduce fairly well the characteristic distribution of FRM having the gradient across the jet axis (Perley, Bridle, & Willis 1984, Asada et al. 2002, Gabuzda & Murray 2003). The systematic FRM gradient was caused by the gradient of the line-of-sight component of the magnetic field. This means that the existence of the helical magnetic field (and the propagation of TAWs) is plausible. On the basis of this success, in this paper the treatment is advanced to the non-axisymmetric situation, the wiggled structure, in AGN jets.

The morphological structures in AGN jets, such as "wiggles (kinks)" or "bends" are frequently seen not only on kpc scales, but also on pc scales and smaller (Hummel et al. 1992). Such a helical distortion might be caused either by plasma instabilities or precession of jet ejection axis due to the gravitational interaction between binary Black Holes (BBHs) (Begelman, Blandford, & Rees 1980), BH/disk, or galaxies. Magnetically driven jets possess a toroidal field component, which is equivalent to an axial electric current, and such "current-carrying" jets are susceptible to MHD instabilities, and moreover, Kelvin-Helmholtz instabilities must be also taken into account for jet dynamics. MHD instabilities are usually divided into pressure-driven instabilities and current-driven instabilities (Bateman 1980). Kelvin-Helmholtz instabilities have been considered for past decades by many theoretical and numerical work (for reviews, see Birkinshaw 1991; Ferrari 1998, and references therein). One of the promising possibilities is a magnetic mechanism based on the "sweeping magnetic twist model". It was shown by 3-dimensional MHD simulations that the formation of the wiggled structure can be explained by the current-driven helical kink instability (Todo et al. 1993). In these simulations, the magnetic field was a force-free helical field from the beginning and the propagation of TAWs was not dealt with. Nakamura, Uchida, & Hirose (2001) extended the treatment of the "sweeping magnetic twist model" to the part far from the gravitator and the accretion disk. They investigated the behavior of TAWs propagating far from the AGN core. They showed that the current-driven helical kink instability can explain the production of the observed wiggles. If the mechanism of the wiggle formation is clarified, it can become a clue to the physics of the jet formation.

In this paper, we calculate FRM, the projected magnetic field, and the total intensity from the numerical data of a MHD simulation based on our "sweeping magnetic twist model", and discuss these model counterparts comparing with an observation. Here we consider the wiggled structure of the jet, and thus use the same kind of 3-dimensional simulation as in Nakamura et al. (2001). In section 2, we describe the application of the model to the distant part of the jet from the AGN core, and show the formation of a helical structure of the jet by the current-driven helical kink instability. We introduce the method to calculate model counterparts of observational quantities in section 3, and show the results in section 4. We discuss comparison between the calculated distributions and observed ones in section 5. The conclusion is summarized in section 6.

2. Numerical Simulation

The “sweeping magnetic twist model” was proposed for star-forming jets (Uchida & Shibata 1985, Shibata & Uchida 1986), and it has since then been extended to the case of AGN jets (Uchida & Shibata 1986, Matsumoto et al. 1996, Uchida et al. 1999, Uchida et al. 2000, Nakamura et al. 2001) as described in paper I in some detail. In paper I, we confined ourselves to the straight part of the jet as a first step, by using the 2-dimensional axisymmetric model. In the present paper, we extend our treatment to the wiggled part of our 3-dimensional jet model, in order to compare the model counterpart with the observation. In this section, we describe the formation of the wiggled structure due to the current-driven helical kink instability.

2.1. Brief Explanation of the Model — Assumptions and Basic Equations

Figure 1 is the schematic picture of a physical situation we treat in this paper. We consider a primordial large scale magnetic field, and that it is squeezed under an assumption of frozen-in magnetic flux due to the gravitational contraction to form the central AGN core (Figure 1a, b). During the contracting process of the magnetized gas, the toroidal component of the magnetic field is continuously created by the rotation of the intergalactic medium having the angular momentum. As a result, large amplitude non-linear torsional Alfvén waves (TAWs) begin to propagate out along the large scale poloidal field. We expect that this process reaches its maximum as the accretion disk is formed, and the interaction of the rotating accretion disk and the poloidal magnetic field penetrating it reaches its maximum phase (Figure 1c). And also, the MHD jets powered by TAWs are emitted in opposite directions along the rotation axis of the disk which is the direction of the original large scale poloidal magnetic field.

In the present paper, we concentrate our attention on the distant part of the jet from the AGN core. The TAWs finally encounter the ambient medium with a higher density surrounding the large spherical “cavity” from which the mass fell toward the center in the gravitational contraction (Figure 1d). The HST optical and MERLIN radio observations of a few hundreds pc-scale 3C264 jet indicate that the jet has a wiggled structure as a result of interacting with a circular optical cold (dense) “ring”, which may be a true ring, a shell, or a filled spheroid (Baum et al. 1997). This observational result indicates the interaction between the jet and the ambient medium will affect the jet dynamics and morphology. The existence of denser material ahead of the propagating TAWs causes the deceleration of MHD jets due to the decreasing local Alfvén velocity; the accumulation of the toroidal component of the magnetic field occurs, which may lead to the current-driven helical kink instabilities through this non-linear process (Nakamura et al. 2001). Even in the case of decreasing density atmospheres, the MHD jets would be subject to the current-driven kink distortions (M. Nakamura & D. L. Meier, in preparation).

The computational domain we report here is also shown in Figure 1(d), and it includes a part of “squeezed” poloidal field near the edge of the density “cavity”. We assume the poloidally mag-

netized intergalactic medium with a varying Alfvén velocity distribution (*i.e.*, gradually decreasing as the TAWs propagate) due to the existence of a denser shell which represents the edge of the ”cavity” . A continuous cylindrical MHD inflow, powered by TAWs into the ”evolved” region of the domain, is specified for all time in the lower ”boundary zone”. We note that a quasi-stationary Poynting-flux-dominated flow is injected into our calculated region throughout the time evolution.

We adopt the ideal MHD as the governing equations.

$$\frac{\partial \rho}{\partial t} + \nabla \cdot (\rho \mathbf{v}) = 0 \quad (1)$$

$$\rho \frac{\partial \mathbf{v}}{\partial t} + \rho (\mathbf{v} \cdot \nabla) \mathbf{v} + \nabla p - \frac{1}{4\pi} (\nabla \times \mathbf{B}) \times \mathbf{B} = 0 \quad (2)$$

$$\frac{\partial p}{\partial t} + \nabla \cdot (p \mathbf{v}) - (1 - \gamma) p \nabla \cdot \mathbf{v} = 0 \quad (3)$$

$$\frac{\partial \mathbf{B}}{\partial t} - \nabla \times (\mathbf{v} \times \mathbf{B}) = 0 \quad (4)$$

where ρ, p, \mathbf{v} are the density, pressure, and velocity of the gas, and \mathbf{B} is the magnetic field. γ represents the ratio of specific heats and is equal to 5/3 in this paper. In paper I, we introduced the effect of gravity in eq. (2) in order to consider the launching and accelerating of MHD jets near the AGN core. We neglect the gravity term in this equation, and concentrate on the dynamics of the propagating MHD jets in this paper. We normalize all physical quantities by the typical Length L_0 , typical density ρ_0 , and typical velocity V_0 . L_0 is ten times as long as the radius with the maximum velocity of the circular motion. ρ_0 and V_0 are the density and the Alfvén velocity at the origin respectively. The total computational domain is taken to be $x_{\min} \leq x \leq x_{\max}$, $y_{\min} \leq y \leq y_{\max}$, and $z_{\min} \leq z \leq z_{\max}$, where $x_{\min} = y_{\min} = -5.10$, $x_{\max} = y_{\max} = 5.10$, $z_{\min} = -1.00$, and $z_{\max} = 12.09$. The numbers of grid points in the simulation reported here are $(N_x \times N_y \times N_z) = (243 \times 243 \times 655)$, where the grid points are distributed non-uniformly in the x, y , and z directions. The grid spacing is uniform, $(\Delta x, \Delta y, \Delta z) = (0.015, 0.015, 0.015)$ for $|x| \leq 0.99$, $|y| \leq 0.99$, and $z \leq 8.0$, and then stretched by 5 % per each grid step for the regions $|x| > 0.99$, $|y| > 0.99$, and $z > 8.0$.

Initial conditions are almost the same as those of Nakamura et al. (2001), but the radial profiles of V_ϕ and V_z (the circular motion and inflow imposed at the lower ”boundary zone”) in this paper are different from those in Nakamura et al. (2001). The profiles in this paper are shown in Figure 2. The initial distributions of the density and the pressure of the gas, and the 3-dimensional configuration of selected magnetic lines of force, are shown in Figure 3. This figure displays the distributions of the range of $-1.0 \leq y \leq 1.0$, $0.0 \leq z \leq 8.0$. B_z decreases gradually along the z -axis and tend to $\sim z^{-2}$ for the upper region, and ρ also decreases in the same way, but increases again toward the upper boundary. We assume a constant pressure throughout the computational domain and the plasma β (the ratio of gas pressure to magnetic pressure) at the origin is 0.01. The value of the plasma β increases along the z -axis and exceeds unity at $z = 3.8$. In the decreasing region (ρ and B) in the lower part, we have the constant Alfvén velocity ($V_A \equiv |B|/\sqrt{\rho}$), and gradually decreasing distribution of V_A as ρ increases. The formation of the wiggled structure is

universal independent of the imposed velocity profiles. The clearest difference in the results between Nakamura et al. (2001) and this paper is the time which it takes before the wiggled structure is formed.

2.2. Time evolution

We discuss the dynamical behavior of a typical case in our performed 3-dimensional simulations: the growth of a current-driven instability in a MHD jet. Figure 4, 5, and 6 show the time evolution of the density, pressure, and 3-dimensional configuration of the selected magnetic lines of force in the $y - z$ plane ($-1.0 \leq y \leq 1.0$, $0.0 \leq z \leq 8.0$) at $x = 0.0$. In the early stage ($t = 3.0$), a strongly magnetized helical jet powered by TAWs advances with a constant velocity into the decreasing poloidally magnetized medium. Our MHD jets have a fast-mode MHD wave front, and a slow-mode MHD wave front closely beyond a contact surface. The front of the TAW (a fast-mode MHD wave) begins to be decelerated due to the gradually decreasing V_A ; the accumulation of B_ϕ occurs behind this wave front ($t = 10.0$). The toroidal magnetic pressure gradient force $d(B_\phi^2/2)/dz$ becomes large and works effectively at this front, strongly compressing the external medium along this propagating TAW front. The initially "hourglass-shaped" magnetic field becomes "tucked up" behind this wave front ($t = 15.0$). At later stages the front becomes super-fast magnetosonic and a strong bow shock (fast-mode MHD shock) is formed. The accumulation of B_ϕ causes a concentration of the axial current density J_z near the central (z) axis (Figure 7 *left*), and the magnetic pitch ($|B_\phi/rB_z|$) becomes large inside the jet. The Lorentz force breaks the quasi-equilibrium balance in the radial direction, and the jet is disrupted ($t = 19.0 - 20.0$). We have an asymmetric distribution of the current density and projected (in a $x - y$ plane) velocity field seen in Figure 7 *right*. There is a strong correlation between the 3-dimensional configuration of the magnetic field and the distribution of specific power due to the radial (r) component of the Lorentz force: $-J_z B_\phi V_r / \rho + J_\phi B_z V_r / \rho$ (Figure 8). Therefore it is confirmed that the distortion of our MHD jet is driven by the current-driven helical kink instability ($m = 1$) (Nakamura et al. 2001).

3. Method of Calculation of Model Counterparts

Using the numerical data of the 3-dimensional simulation explained in the previous section, we computed the distributions of FRM, the projected magnetic field, and the total intensity seen from different viewing angles.

We computed the FRM distribution by integrating B_\parallel along the line-of-sight although in paper I we integrated $n_e B_\parallel$. In this paper, we intend to consider the effect of the deformed magnetic field configuration and to omit the effect of the dense shell from consideration. To calculate Stokes parameters, we assume the following: (1) radiation processes are dominated by synchrotron radiation, (2) synchrotron self absorption is negligible, (3) the spectral index, α , is equal to unity, and

(4) the projected magnetic field is perpendicular to the projected electric field. The emissivity of the synchrotron radiation is given by $\epsilon = p|B \sin \psi|^{\alpha+1}$, where B is the local magnetic field strength, ψ is the angle between the local magnetic field and the line-of-sight, and p is the gas pressure. In our simulation the relativistic particles are not explicitly tracked, therefore we assume that the energy and number densities of the relativistic particles are proportional to the energy and number densities of the thermal fluid (Clarke et al. 1989, Hardee & Rosen 1999, 2002). The total intensity is then given by the integration of the emissivity along the line-of-sight as $I = \int \epsilon ds$. Other Stokes parameters are given by $Q = \int \epsilon \cos 2\chi' ds$ and $U = \int \epsilon \sin 2\chi' ds$, where the local polarization angle χ' is determined by the direction of the local magnetic field and the direction of the line-of-sight. Using these U and Q , the polarization angle χ is given by $\chi = (1/2) \tan^{-1}(U/Q)$. Finally the projected magnetic field is determined from the polarization angle χ and the polarization intensity $\sqrt{Q^2 + U^2}$.

Here we separate the Faraday rotation screen and the emitting region, and we performed the integrations only in the emitting region for Stokes parameters, and only in the Faraday rotation screen for FRM. We assumed this separation on the basis of the fact that linear dependence of the observed polarization angle on wavelength-squared holds in some observations (Perley et al. 1984, Feretti et al. 1999, Asada et al. 2002, Gabuzda & Murray 2003); this would not be the case if the Faraday rotation is caused in the emitting region (Burn 1966). The emitting region and the Faraday rotation screen are deformed into the 3-dimensional shape in the helical kink instability. Therefore we trace the flux tube in its time development by the initial footpoints of magnetic lines of force at the upper boundary of the simulation region. This is reasonable because the footpoints don't move until a wave front arrives. The region which is defined as the Faraday rotation screen is almost corresponding to the magnetic tube to which the circular motion is imposed.

4. Results of the Numerical Observation

4.1. Before the formation of the wiggled structure

Figure 9 shows the FRM distributions at the time before the formation of the wiggled structure ($t = 15.0$). Black in the map corresponds to a maximum and white to a minimum in each viewing angle case. The FRM distributions have the gradient in the direction perpendicular to the jet axis independent of the viewing angle. This gradient is caused by the toroidal magnetic field propagating as TAWs.

Figure 10 shows the total intensity distributions. When the angle between the jet axis and the line-of-sight, θ , is equal to 90° , total intensity has the highest value on the jet axis since both the emissivity and the integration depth of the emitter are maximum. As the viewing angle becomes small, the asymmetry appears owing to the asymmetry of the emissivity, this is equivalent to the asymmetry of the magnetic field component perpendicular to the line-of-sight. The jet has the helical magnetic field, therefore it is opposite in both sides of the jet whether the emissivity

increases or decreases when the viewing angle changes. Figure 11 shows the distributions of the projected magnetic field. It is parallel to the jet axis in almost all region independent of the viewing angle because the pitch angle of the helical magnetic field is not so large. However, the polarization intensity becomes lower as θ becomes small.

4.2. After the formation of the wiggled structure

The FRM distributions at the time after the formation of the wiggled structure ($t = 20.0$) are shown in Figure 12. The gradient across the jet axis is partly seen, but not seen in the wiggled structure because the toroidal component of the magnetic field is smaller compared to the field component along the structural axis; i.e., the magnetic field is less twisted around the wiggled structure. Therefore FRM is large in the structure coming toward us and small in the structure going backward. This means that the FRM distribution in the wiggled structure can strongly reflect its 3-dimensional shape. FRM changes suddenly where different parts of the wiggled jet overlap each other as seen by the observer.

Figure 13 shows the total intensity distributions. Behind the fast-mode MHD shock front, toroidal magnetic field is accumulated and magnetic field is strengthened. It leads the emissivity to increase and the total intensity to become high. On the other hand, the intensity is not so high in the wiggled structure, where the magnetic field is less twisted around the wiggled structure. However, as the viewing angle becomes small, the intensity in the wiggled structure increases because the structure which lies on this side and that on the back side overlap on the same ray. This means that the integration depth of the emitter increases. For the same reason, the polarization intensity gets higher in the wiggled structure (Figure 14). The projected magnetic field is along the structural axis of the jet on the whole. In the wiggled structure, the projected field appears transverse to the global jet axis (z -axis).

5. Discussion

In this section, we discuss the comparison between the calculated distributions shown in the previous section and those in the 3C449 jet. Figure 15 shows the distributions of FRM and the projected magnetic field in part of the 3C449 jet (Feretti et al. 1999). As we go along the jet, the color in the FRM distribution starts from blue, changes to deep blue, jumps to yellow, and changes to red at an edge of the jet (a bending point) on the right hand side. The parallel projected magnetic field exists widely where the color in the FRM distribution is yellow or red.

Figure 16 shows the color FRM distribution of the Figure 11(c) and the projected magnetic field distribution (θ is equal to 55°) in the wiggled structure. The structure takes the form of a 3-dimensional helix. The structure going backward corresponds to blue, while that coming toward us corresponds to red. The structure going upward almost perpendicularly to the line-of-sight

corresponds to the yellow part. The projected magnetic field in the wiggled structure is almost parallel. This is caused by the following; the structure going from left to right on the back side and that from right to left on this side appear to overlap partly (cf. Figure 17).

As stated in section 3, we omitted the effect of the dense shell from consideration. Here we demonstrate the effect of the dense shell. Figure 18 shows the FRM distribution in the wiggled structure calculated by the integration of $n_e B_{\parallel}$. The characteristics of the distribution are same so that it can be said that the dense shell do not affect the distribution qualitatively so much in this case.

Feretti et al. (1999) estimated the jet velocity and the inclination of the line-of-sight by the ratio of P_{c-obs} to P_{c-exp} , where P_{c-obs} is the really observed core radio power at 5GHz and P_{c-exp} is the power inferred from the total radio power at 408MHz. From such estimation, they concluded that an initial jet velocity is $0.9c$ and a jet inclination to the line-of-sight is 82.5° . However, these values were obtained from the information about near the core. It is likely that the jet is bent in some places. Birkinshaw, Laing, & Peacock (1981) estimated from the polarization intensity along the jet that the inclination of the north jet in 3C449 is 53° . This inclination is almost same with that at which we can reproduce the characteristics of the observation.

These similarities between the calculated distributions and the observed ones suggest that the 2-dimensional wiggle in the observation is due to the projection of a 3-dimensional helical structure onto the plane of the sky. It is also suggested that the structure which lies on this side (yellow) hides the structure on the back side. The reddish part corresponds to the part coming toward us in the helix. If this is the case, it is highly likely that the magnetic field (especially the toroidal component) plays an important role not only in the emission but also in the dynamics of the jet formation because the wiggle formation is caused by the accumulation of the toroidal field. It is also suggested that the FRM distribution can be a sensitive clue for telling which of the proposed models is the correct one.

Because it is not obvious that how much the Faraday screen that is irrelevant to the jet itself contributes to the value of rotation measure, it is not possible to predict the value of Faraday rotation measure. It is, however, possible to estimate the difference between the maximum and the minimum of rotation measure. In our simulation, the scale of the wiggled structure is almost equal to the length unit of the simulation. Integration depth of Faraday screen is about twice as long as the length unit. The rotation measure is given by $\text{FRM} [\text{rad m}^{-2}] = 8.1 \times 10^5 n_e [\text{cm}^{-3}] B_{\parallel} [\text{G}] L_{FS} [\text{pc}]$, where n_e is the electron density, B_{\parallel} is the line-of-sight component of the magnetic field and L_{FS} is the integration depth of the Faraday screen. In our calculation, L_{FS} is twice as long as L_{wiggle} where L_{wiggle} is the scale of the wiggled structure. If the maximum of the rotation measure (FRM_{max}) is made by $B_{\parallel} = \langle B \rangle$ and the minimum of the rotation measure (FRM_{min}) by $B_{\parallel} = -\langle B \rangle$, then $\text{FRM}_{max} - \text{FRM}_{min} = 3.2 \times 10^6 n_e \langle B \rangle L_{wiggle}$. In the case of 3C449 jet, the scale of the wiggled structure is about $1'$ (from $39^\circ 07'$ to $39^\circ 08'$ in Figure 15) and it corresponds to 30kpc. Finally $\text{FRM}_{max} - \text{FRM}_{min}$ is equal to $9.8 \times 10^{10} n_e \langle B \rangle$. In the case of 3C449 jet, FRM_{max}

- FRM_{\min} is nearly equal to 100 [rad m⁻²] (Feretti et al. 1999). It is therefore predicted from our calculation that $n_e \langle B \rangle$ in the jet is equal to 10⁻⁹ [G cm⁻³].

Except for the wiggled structure, there are some differences. First, the total and polarized intensities enhance beyond the wiggled structure in the model counterparts while it is not seen in the observation. The enhancement of the intensities in the model counterparts is due to the accumulation of the toroidal magnetic field. This is equivalent to the enhancement of the current density. It is therefore likely that the magnetic reconnection takes place. The magnetic reconnection is the dissipation of the magnetic field so that the strength of the magnetic field decreases and the intensities can also decrease. For more exact discussion, resistive MHD simulations are necessary. Second, the projected magnetic field is longitudinal at the side near the core in the model counterparts while it is transverse in the observation. It is remarkable that the transverse field was obtained in paper I in which the part of the jet near the core was dealt with. We therefore think that the simulations simultaneously solving the formation, propagation and destabilization of the jet are necessary.

It can be said that the influence of the establishment of the validity of the magnetic model, especially the “sweeping magnetic twist model”, will be extremely large. This claims that the dynamics of the jet formation, including the collimation and the destabilization in large scale, is due to the operation of the magnetic field. Since there is no local source for this large energy to do the job in the part of the space where the wiggles of the jets are seen (closer to the hotspots at the tip of long jets), the energy should come all the way from the AGN core. We also claim that the energy dumped in the hotspots and the radio lobes is carried by the Poynting flux. In MHD models, the toroidal component is generated and its propagation carries the Poynting energy, therefore the models are plausible. The generation of the toroidal magnetic field may be due to either the rotation of the accretion disk (Blandford & Payne 1982, Uchida & Shibata 1985) or the effect of the rotating black hole (Blandford & Znajek 1977, Koide et al. 2000). This means that the large amount of energy is flowing out from the core part of an AGN (though we can not yet say exactly whether that comes from the inner edge of the accretion disk, or from the black hole). If we accept this, the major bearer of energy flowing out is, even in the AGN core itself, large amplitude TAWs, and even very high Lorentz factor phenomena will be a product of the energetic TAWs.

6. Conclusion

We performed a 3-dimensional MHD simulation based on our “sweeping magnetic twist model”, which was applied to the situation far from the AGN core by Nakamura et al. (2001). In the “sweeping magnetic twist model”, the disk rotation generates the toroidal magnetic field and it propagates into two directions along a large scale magnetic field as torsional Alfvén waves (TAWs). In this paper, the situation TAWs are propagating far from the gravitator was dealt with. It was assumed that there is a lower Alfvén velocity region ahead of the propagating TAWs. The toroidal magnetic field becomes accumulated after TAWs enter the low Alfvén velocity region. This causes

the growth of the current-driven helical kink instability and the wiggled structure is formed.

We also calculated the observational quantities (FRM, Stokes, I , Q , and U parameters) by integrating the numerical data along the line-of-sight. The Faraday rotation screen and the emitting region were defined separately. The integration for FRM was done only in the Faraday rotation screen and that for Stokes parameters only in the emitting region. The projected magnetic field was determined from Q and U .

Before the formation of the wiggled structure, the FRM distribution has a gradient across the jet axis. An asymmetry in the total intensity distribution exists except the case where θ is equal to 90° . Same features are seen in the result of paper I and these features can explain some observations (Perley et al. 1984, Asada et al. 2002, Gabuzda & Murray 2003). The projected magnetic field is parallel to the jet axis because the pitch angle of the helical magnetic field is not so large.

After the formation of the wiggled structure, the FRM distribution has a clear correlation with the large scale structure of the jet itself. This is caused by the following; the magnetic field becomes less twisted around the wiggled structure owing to the current-driven helical kink instability. This is equivalent to that the magnetic field is almost along the structural axis of the jet in the wiggled structure. The total and polarization intensities are low in the wiggled structure when the jet inclination to the line-of-sight is large. However, they become higher as the jet inclination becomes small because the structure on the backside and that on the frontside of the 3-dimensional helix overlap on the same ray as seen by observer. We found that when we see the jet at a certain angle, we can reproduce the characteristics of the observation of the 3C449 jet (Feretti et al. 1999). This suggests that the FRM distribution could be strongly affected by the magnetic field in or around the jet and that the jet has a helical structure. If this is the case, it is also suggested that the magnetic field (especially the toroidal component) plays an important role in the formation of astrophysical jets.

Finally, we would like to thank Dr. L. Feretti for providing their precious data of FRM, and for valuable discussions. One of the authors (H. K.) thanks Syuniti Tanuma and Troels Haugbølle for helpful comments. We would hope that more observations of the FRM distribution in AGN jets will be performed in the near future because they are very important and scientifically rewarding. This means that with those we can determine the correct model if our claim in the above is correct. We would therefore urge high quality observations of the FRM distribution, to seek for the clues of the mechanism of jet formation. Numerical computations were carried out on VPP5000 at the Astronomical Data Analysis Center of the National Astronomical Observatory, Japan, which is an interuniversity research institute of astronomy operated by the Ministry of Education, Culture, Sports, Science, and Technology.

REFERENCES

- Asada, K., Inoue, M., Uchida, Y., Kamenno, S., Fujisawa, K., Iguchi, S., & Mutoh, M. 2002, PASJ, 54, L39
- Bateman, G. 1980, MHD Instabilities (Cambridge: MIT Press)
- Baum, S. A., et al. 1997, ApJ, 483, 178
- Begelman, M. C., Blandford, R. D., & Rees, M. J. 1980, Nature, 287, 307
- Birkinshaw, M., Laing, R. A., & Peacock, J. A. 1981, MNRAS, 197, 253
- Birkinshaw, M. 1991, in Beams and Jets in Astrophysics, ed. P. A. Hughes (Cambridge, UK: Cambridge Univ. Press), 278
- Blandford, R. D. 1976, MNRAS, 176, 465
- Blandford, R. D., & Payne, D. G. 1982, MNRAS, 199, 883
- Blandford, R. D., & Znajek, R. L. 1977, MNRAS, 179, 433
- Burn, B. J. 1966, MNRAS, 133, 67
- Clarke, D. A., Norman, M. L., & Burns, J. O. 1989, ApJ, 342, 700
- Eilek, J. A., & Owen, F. N. 2002, ApJ, 567, 202
- Feretti, L., Perley, R., Giovannini, G., & Andernach, H. 1999, A&A, 341, 29
- Ferrari, A. 1998, ARA&A, 36, 539
- Gabuzda, D. C., & Murray 2003, preprint (astro-ph/0309668)
- Hardee, P. E., & Rosen, A. 1999, ApJ, 524, 650
- Hardee, P. E., & Rosen, A. 2002, ApJ, 576, 204
- Hummel, C. A., et al. 1992, A&A, 257, 489
- Koide, S., Meier, D. L., Shibata, K., & Kudoh, T. 2000, ApJ, 536, 668
- Kudoh, T., Matsumoto, R., & Shibata, K. 1998, ApJ, 508, 186
- Laing, R. A. 1981, ApJ, 248, 87
- Lovelace, R. V. E. 1976, Nature, 262, 649
- Matsumoto, R., Uchida, Y., Hirose, S., Shibata, K., Hayashi, M., Ferrari, A., Bodo, G., & Norman, C. 1996, ApJ, 461, 115

- Meier, D. L., Koide, S., & Uchida, Y. 2001, *Science*, 291, 84
- Nakamura, M., Uchida, Y., & Hirose, S. 2001, *New Astronomy*, 6, 61
- Ouyed, R., & Pudritz, R. E. 1997, *ApJ*, 482, 712
- Perley, R. A., Bridle, A. H., & Willis, A. G. 1984, *ApJS*, 54, 291
- Shibata, K., & Uchida, Y. 1986, *PASJ*, 38, 631
- Stone, J. M., & Norman, M. L. 1994, *ApJ*, 433, 746
- Taylor, G. B. 1998, *ApJ*, 506, 637
- Todo, Y., Uchida, Y., Sato, T., & Rosner, R. 1993, *ApJ*, 403, 164
- Uchida, Y., & Shibata, K. 1985, *PASJ*, 37, 515
- Uchida, Y., & Shibata, K. 1986, *Can.J.Phys.*, 64, 507
- Uchida, Y., Nakamura, M., Hirose, S., & Uemura, S. 1999, *Ap&SS*, 264, 195
- Uchida, Y., Nakamura, M., Miyagoshi, T., Kobayashi, T., Mukawa, T., & Hirose, S. 2000, in *IAU Symp. 195, Highly Energetic Physical Processes and Mechanisms for Emission from Astrophysical Plasmas*, ed. P. C. H. Martens, & S. Tsuruta (San Francisco: ASP), 213
- Uchida, Y., Kigure, H., Hirose, S., Nakamura, M., & Cameron, R. 2004, *ApJ*, 600, 88
- Ustyugova, G. V., Koldoba, A. V., Romanova, M. M., Chechetkin, V. M., & Lovelace, R. V. E. 1995, *ApJ*, 439, L39

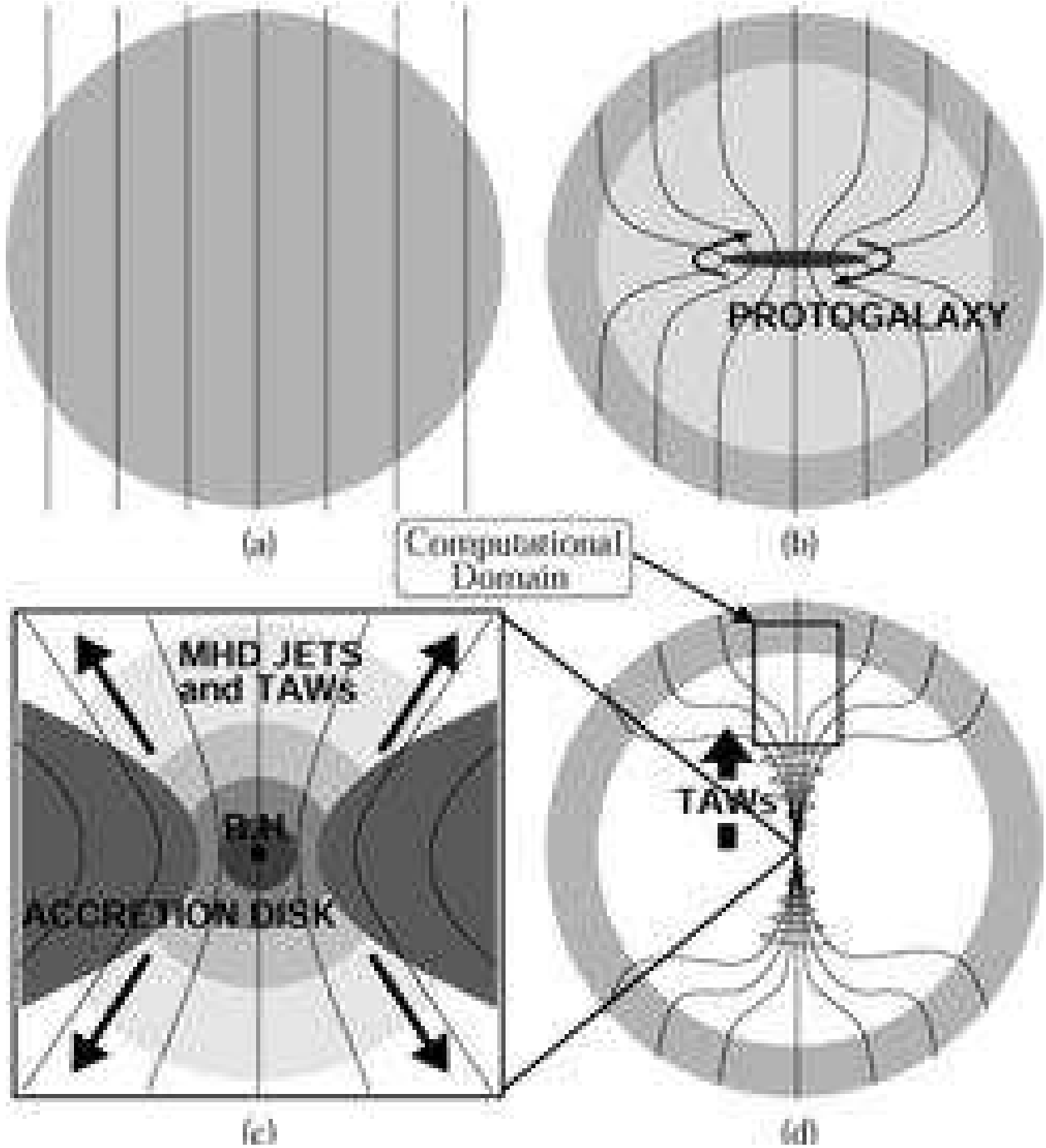


Fig. 1.— Schematic picture of our model. (a) From the intergalactic medium with a large scale magnetic field, (b) the AGN core region and the disk are formed due to the gravitational contraction of mass with the magnetic flux conserved. (c) Torsional Alfvén waves generated by the interaction between the accretion disk and the large scale magnetic field (d) propagate along the magnetic field. The computational domain which we assumed is shown.

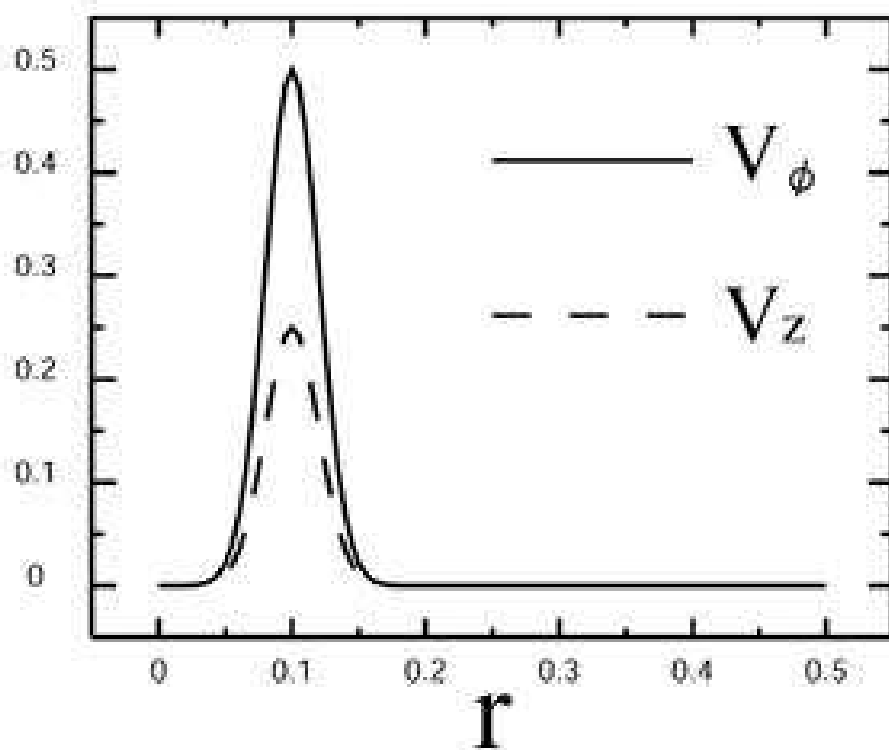


Fig. 2.— The radial profile of imposed circular motion (solid line) and inflow (dotted line) at the lower boundary

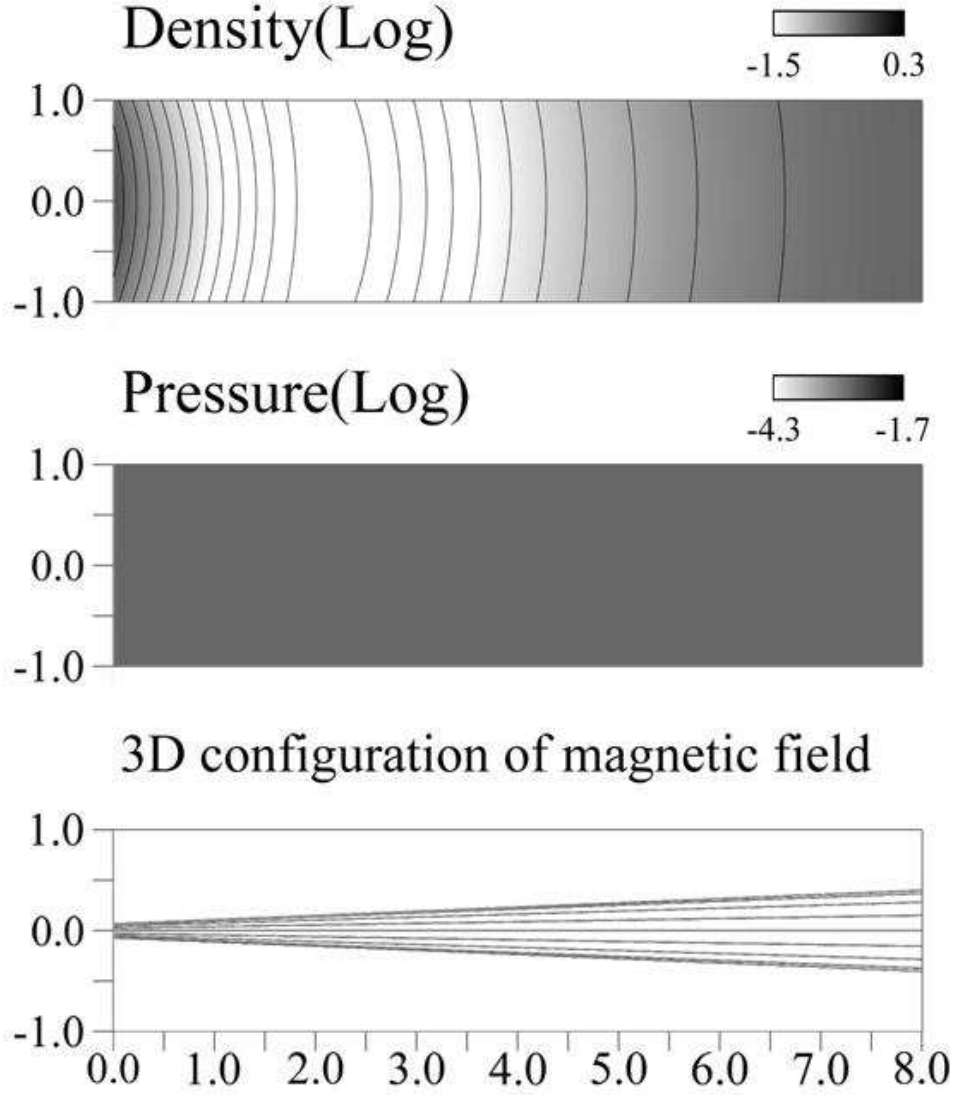


Fig. 3.— The initial distributions of (a) the density, (b) the pressure (initially constant) on the $y - z$ plane ($-1.0 \leq y \leq 1.0$, $0.0 \leq z \leq 8.0$) at $x = 0.0$, and (c) the projected 3-dimensional configuration of the initial magnetic field.

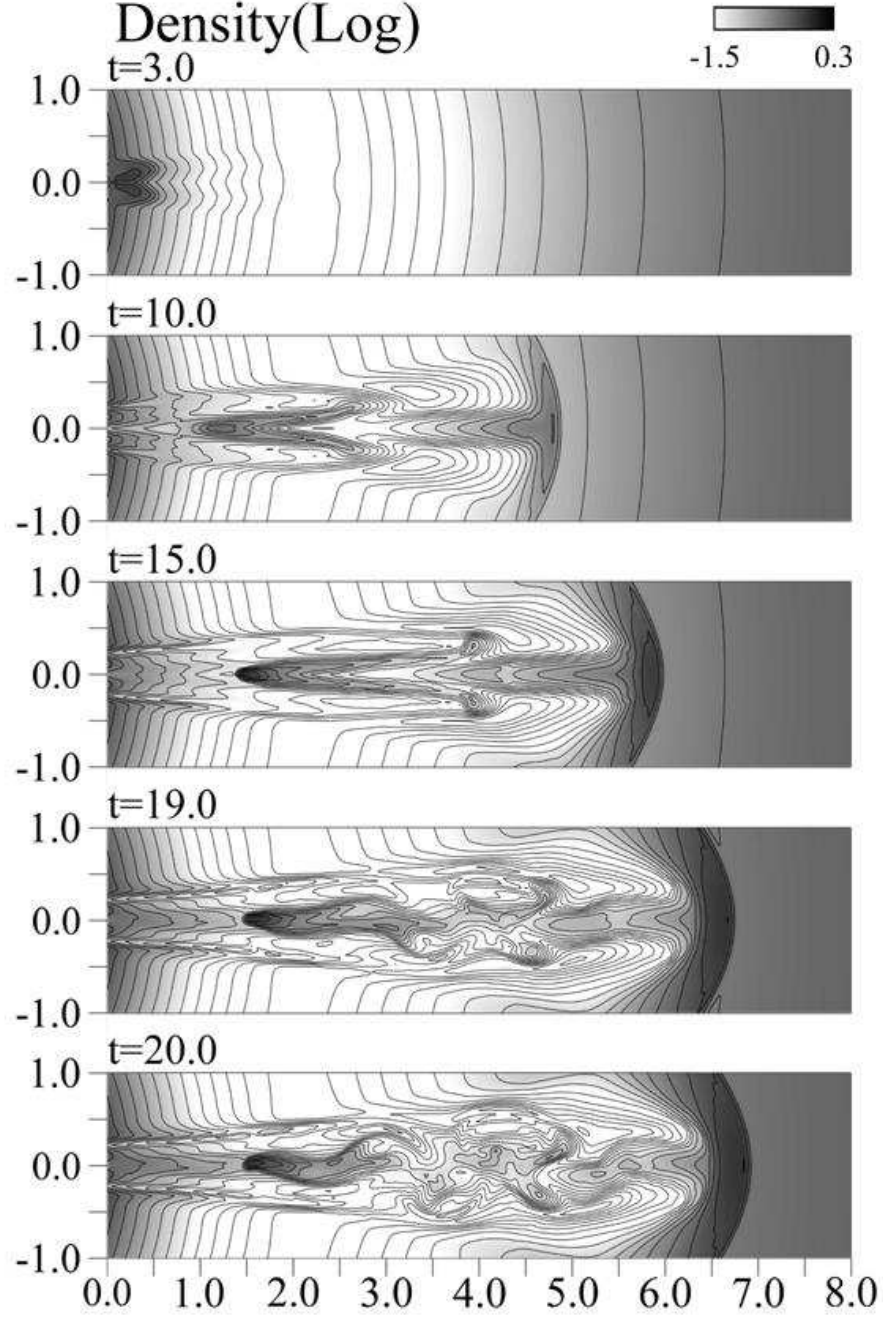


Fig. 4.— Time evolution of the density on the $y-z$ plane at $x = 0.0$ ($-1.0 \leq y \leq 1.0$, $0.0 \leq z \leq 8.0$).

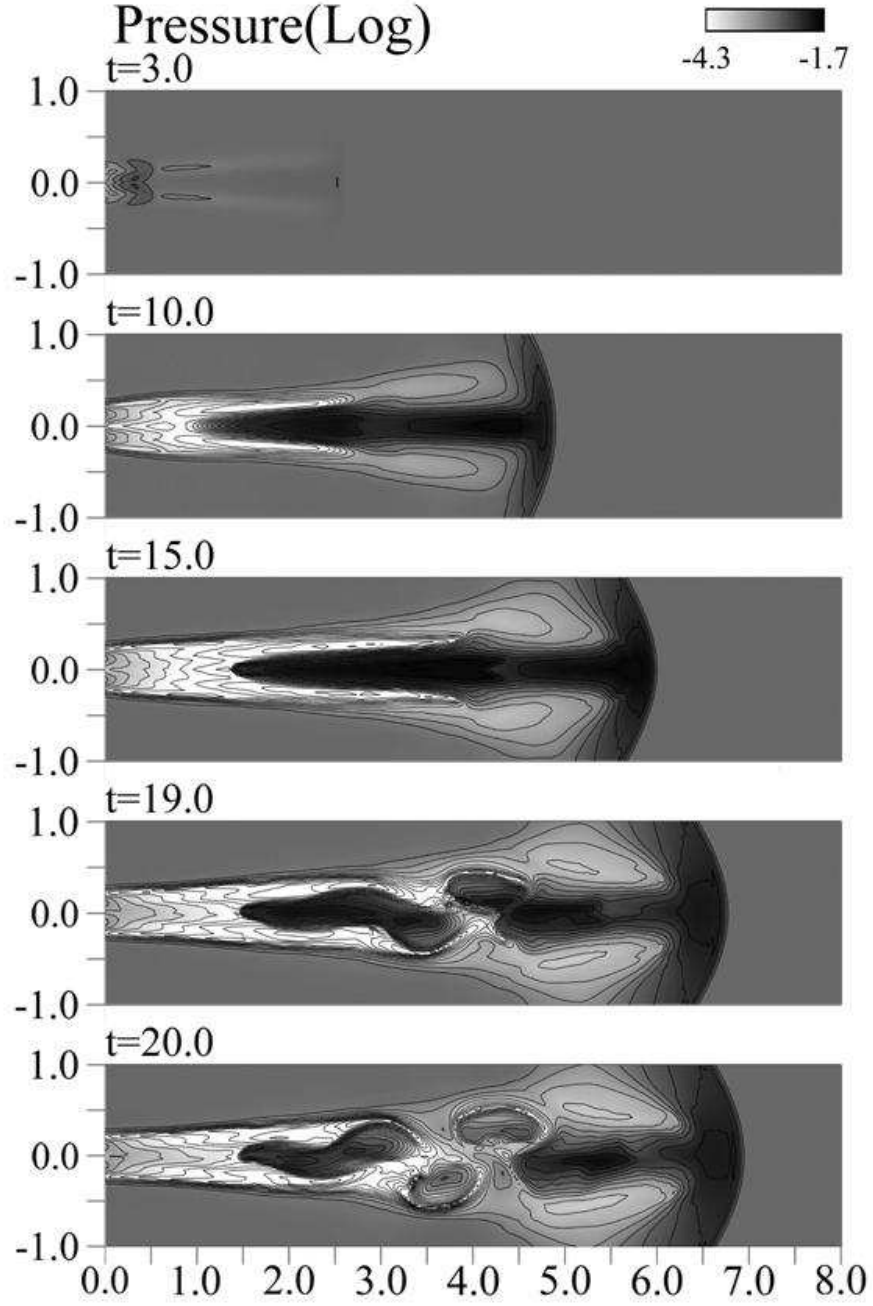


Fig. 5.— Time evolution of the pressure on the $y-z$ plane at $x=0.0$.

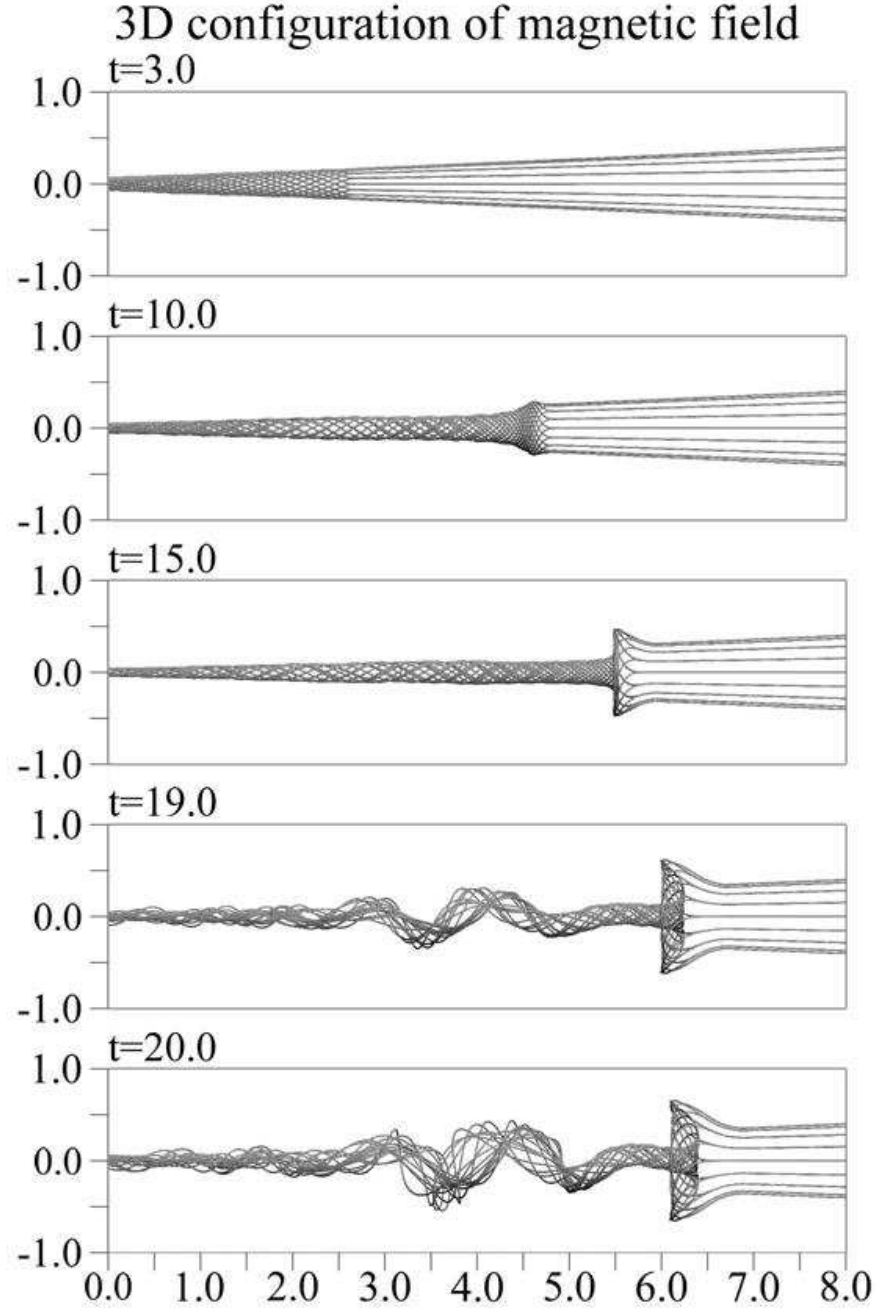


Fig. 6.— Time evolution of the projected 3-dimensional configuration of selected magnetic lines of force.

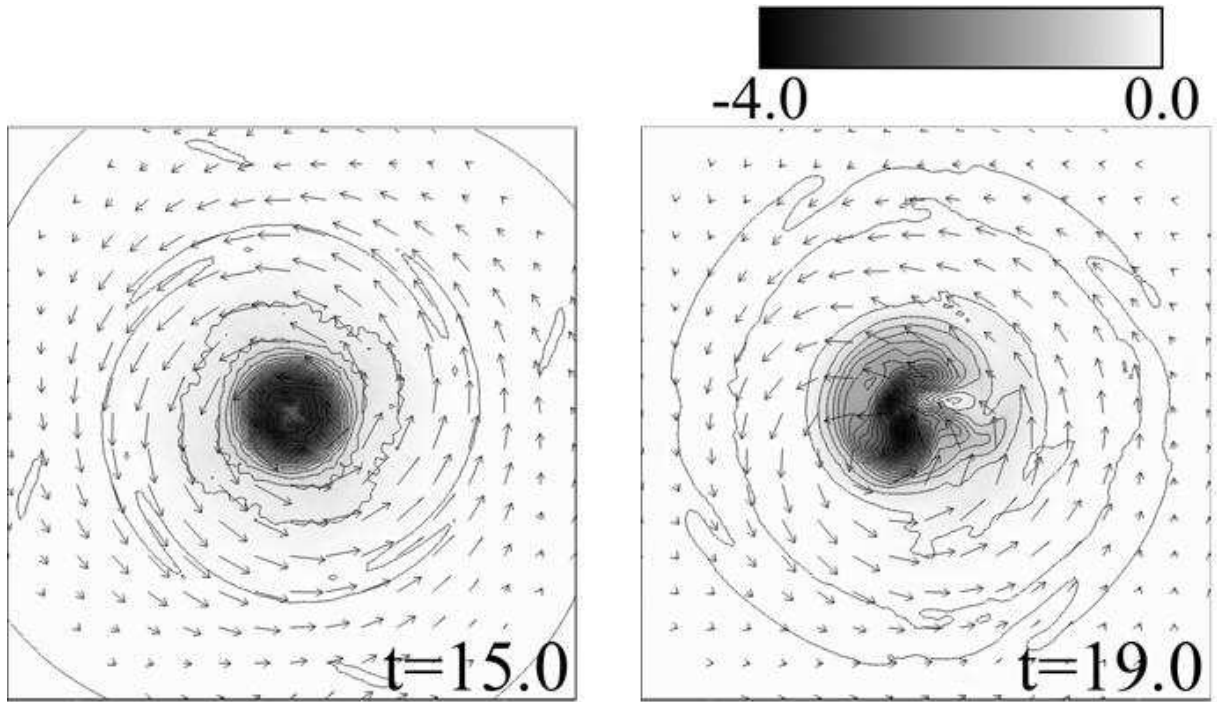


Fig. 7.— Distribution in the $x-y$ plane at $z = 4.25$. A grayscale and contour show the z -component of the current density and arrows show the velocity field.

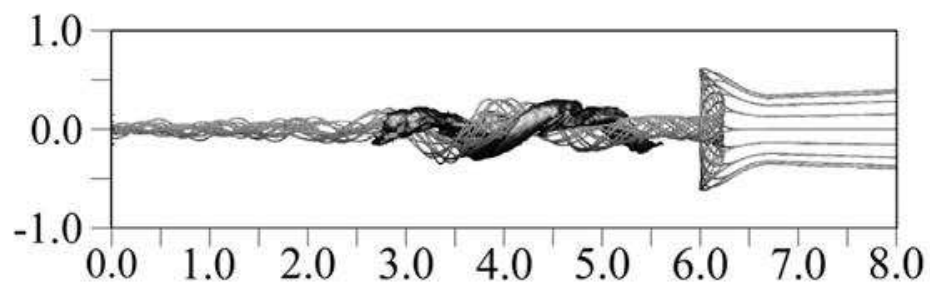


Fig. 8.— 3-dimensional distributions of a typical iso-value surface of the specific power: $-J_z B_\phi V_r / \rho + J_\phi B_z V_r / \rho$ and the selected magnetic lines of force at $t = 19.0$.

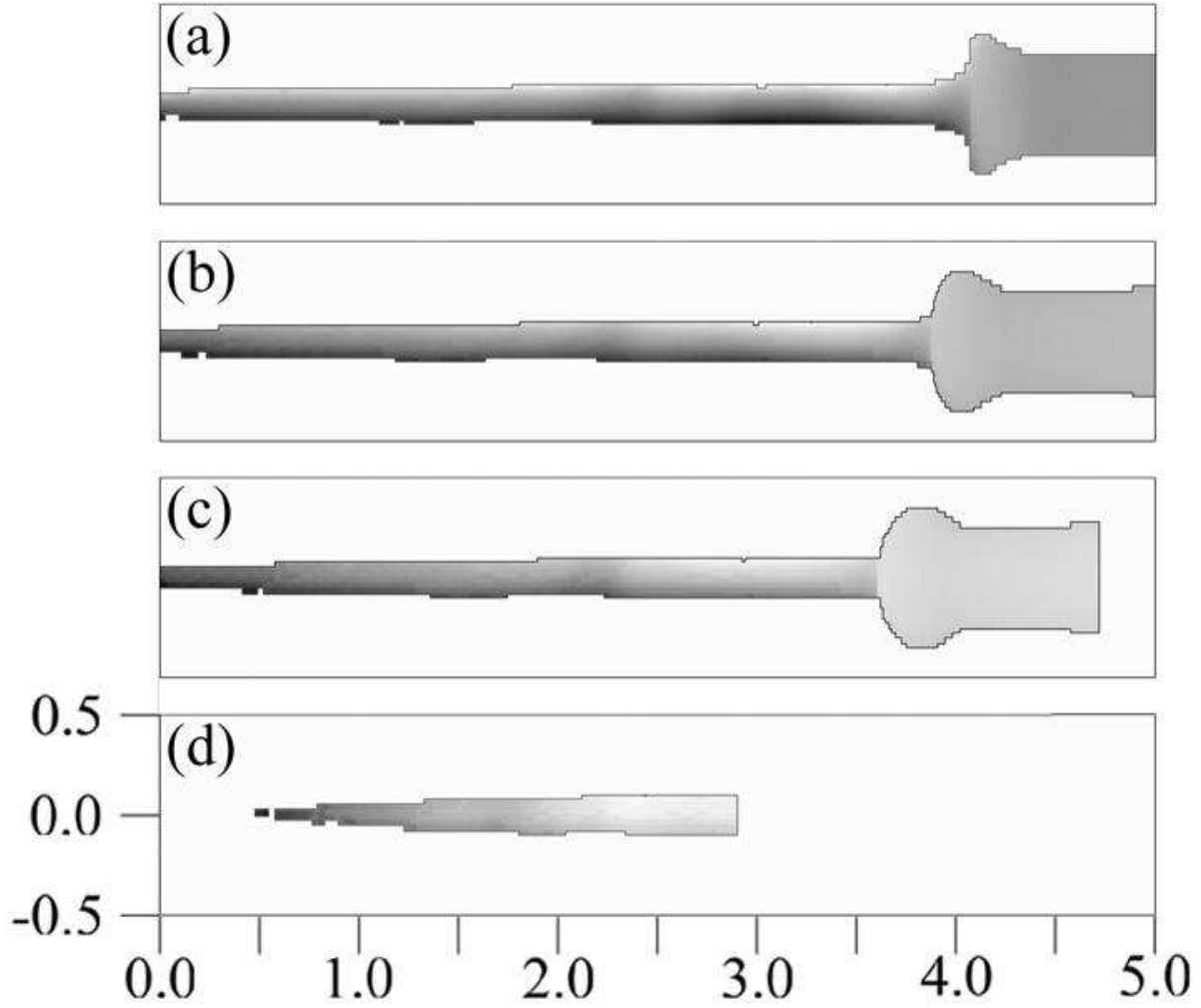


Fig. 9.— Calculated model counterparts for the Faraday rotation measure distribution, when seen at (a) 90° , (b) 70° , (c) 55° , and (d) 30° , from the axis (ahead of the jet) at the time before the formation of the wiggled structure ($t = 15.0$). The data of the numerical observation exists inside the area surrounded by the black line.

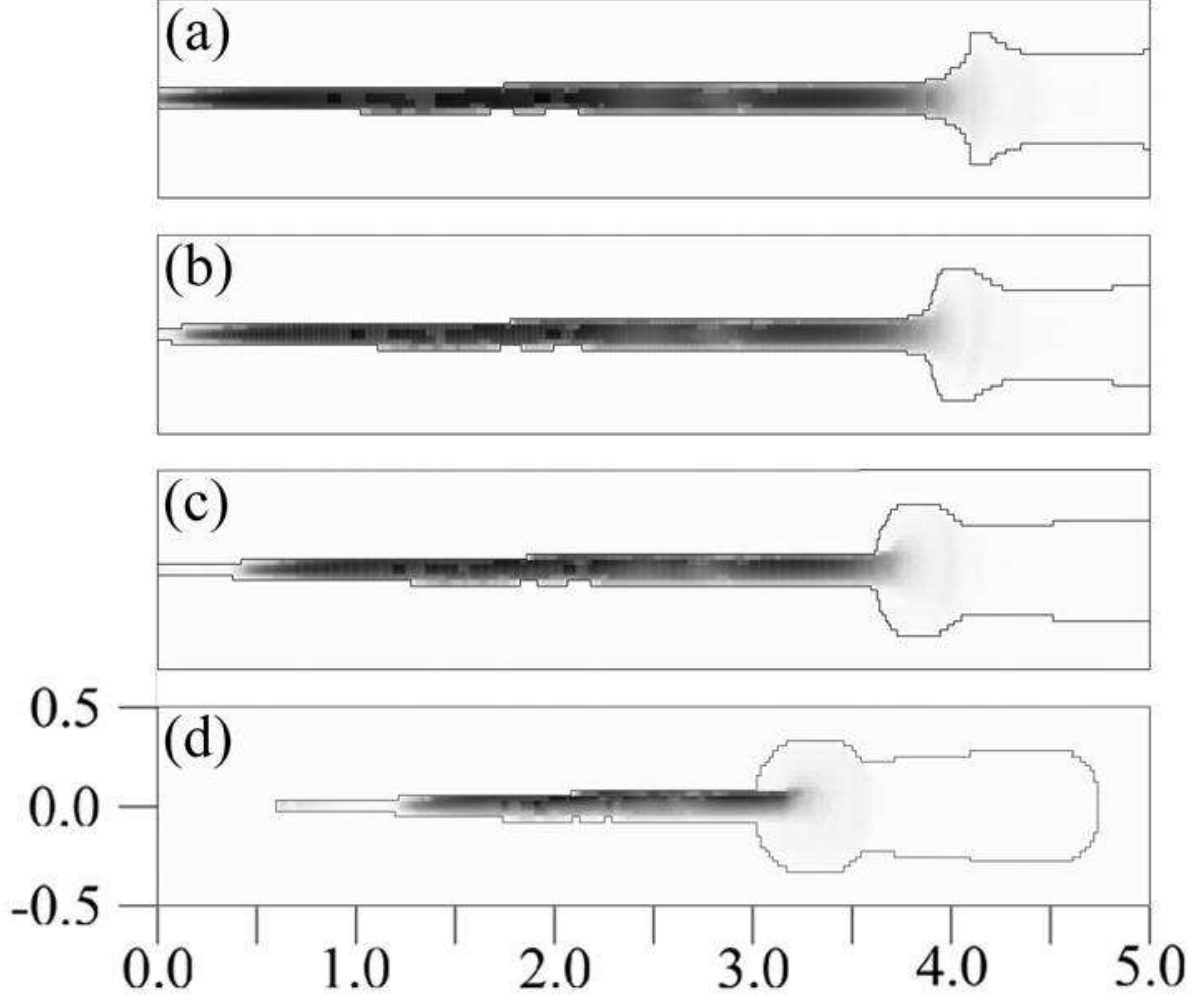


Fig. 10.— Calculated model counterparts for the total intensity, when seen at (a) 90° , (b) 70° , (c) 55° , and (d) 30° , from the axis at $t = 15.0$. The data of the numerical observation exists inside the area surrounded by the black line.

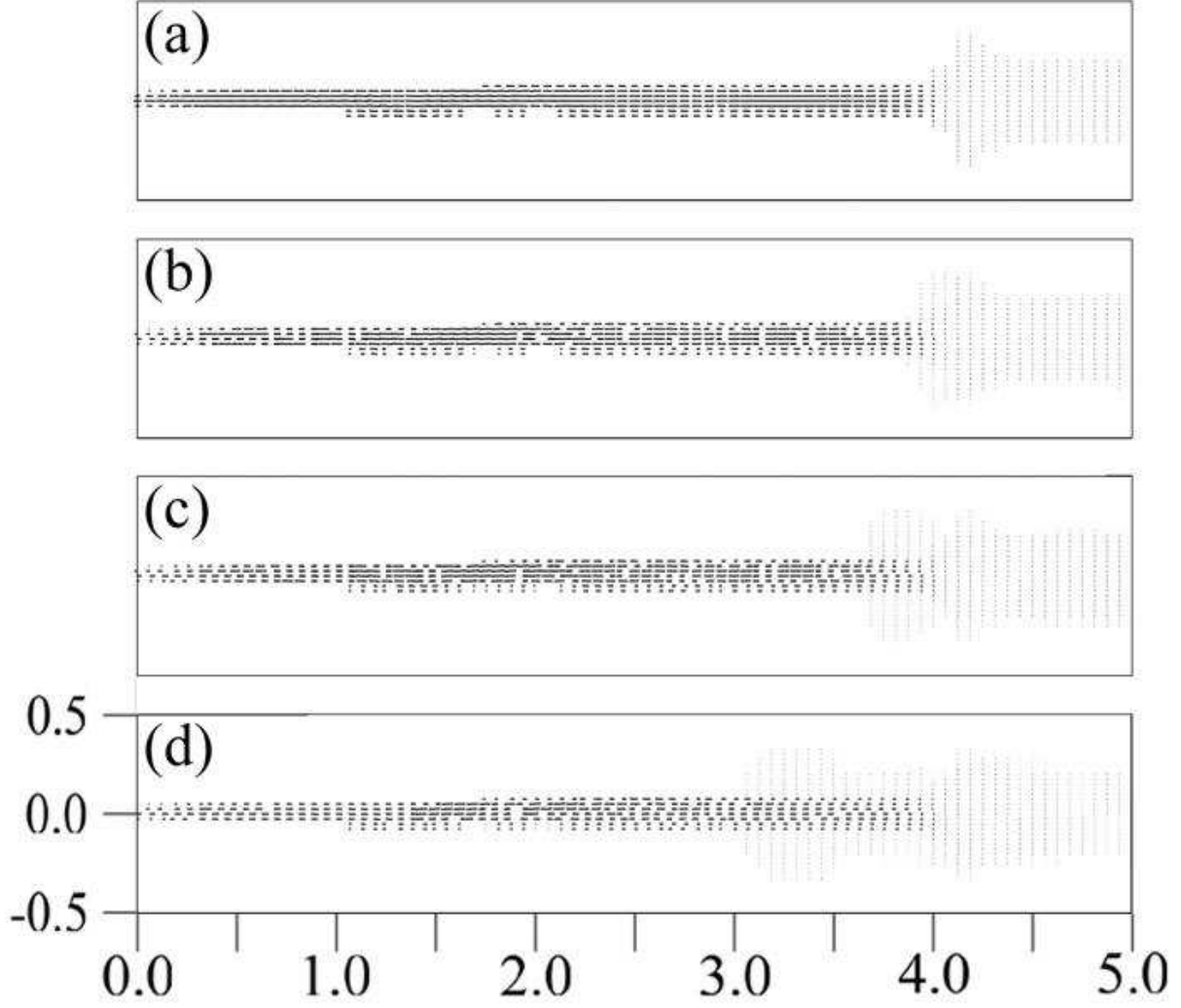


Fig. 11.— Calculated model counterparts for the projected magnetic field, when seen at (a) 90° , (b) 70° , (c) 55° , and (d) 30° , from the axis at $t = 15.0$. The bars represent the direction of the projected magnetic field and the length of the bars represents the polarization intensity.

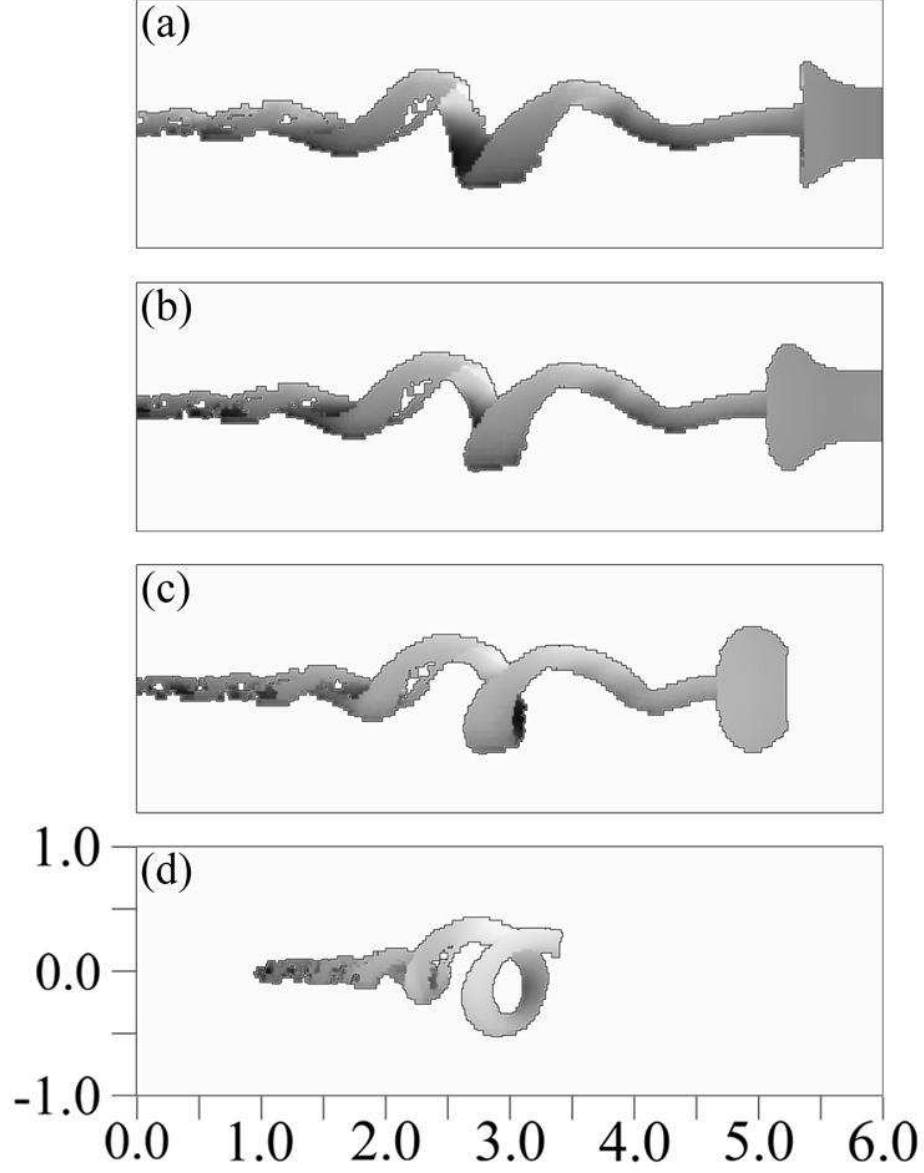


Fig. 12.— Calculated model counterparts for the Faraday rotation measure distribution, when seen at (a) 90° , (b) 70° , (c) 55° , and (d) 30° , from the axis (ahead of the jet) at the time after the formation of the wiggled structure ($t = 20.0$). The data of the numerical observation exists inside the area surrounded by the black line.

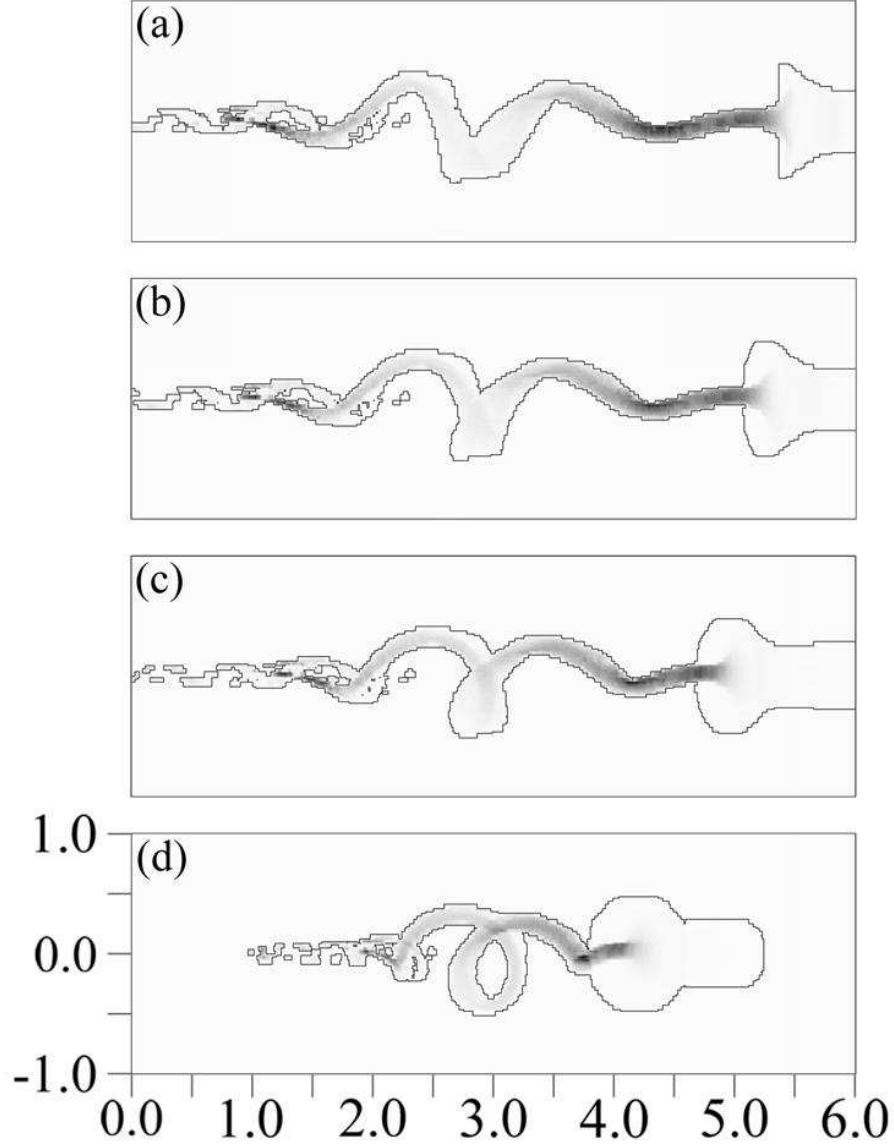


Fig. 13.— Calculated model counterparts for the total intensity, when seen at (a) 90° , (b) 70° , (c) 55° , and (d) 30° , from the axis at $t = 20.0$. The data of the numerical observation exists inside the area surrounded by the black line.

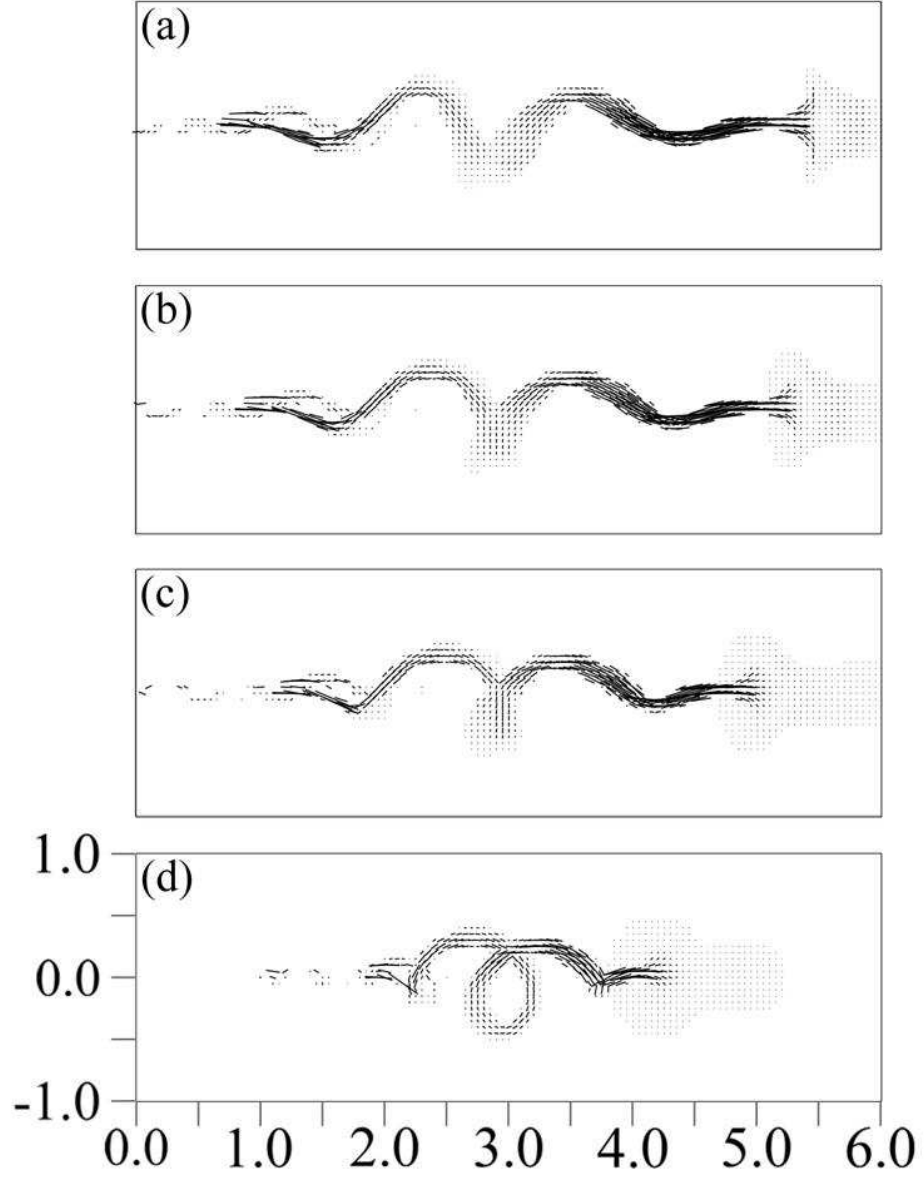


Fig. 14.— Calculated model counterparts for the projected magnetic field, when seen at (a) 90° , (b) 70° , (c) 55° , and (d) 30° , from the axis at $t = 20.0$. The bars represent the direction of the projected magnetic field and the length of the bars represents the polarization intensity.

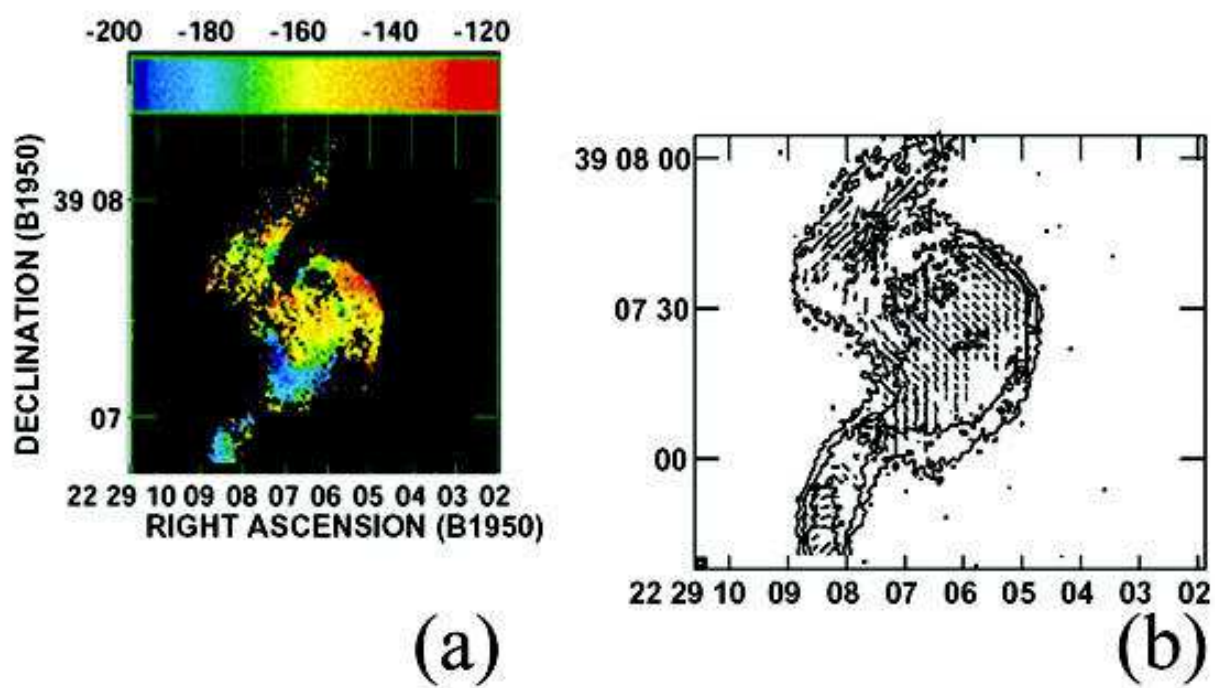


Fig. 15.— The distributions of (a) Faraday rotation measure and (b) the projected magnetic field in part of the 3C449 jet (Feretti et al. 1999).

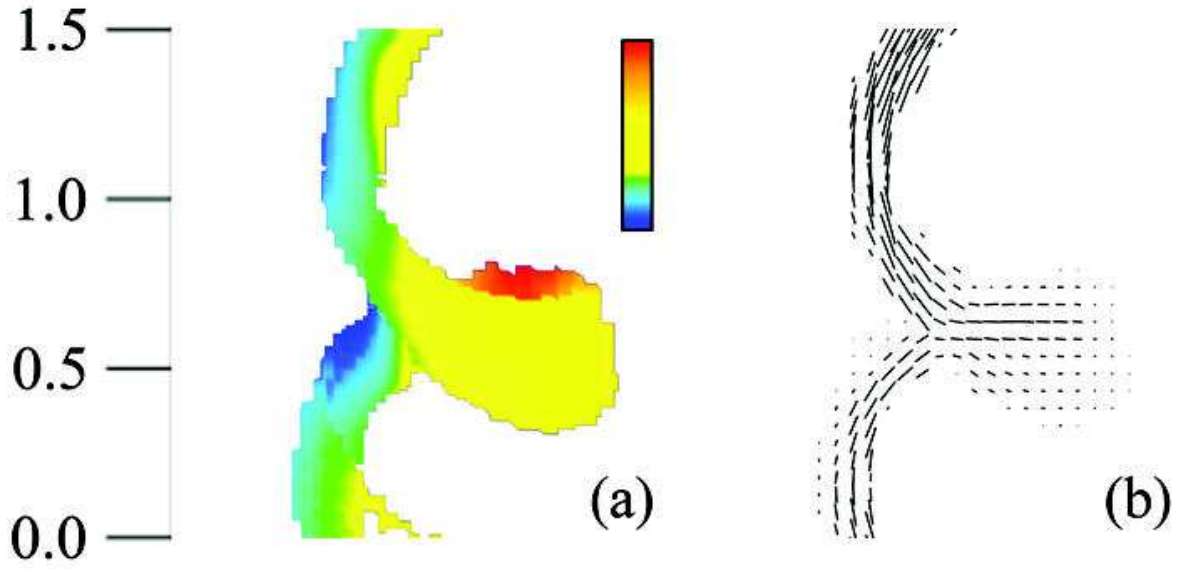


Fig. 16.— The distributions of (a) Faraday rotation measure and (b) the projected magnetic field calculated from the results of the numerical simulation at $t = 20.0$, seen at 55° from the jet axis. In terms of the comparison with the observation of the 3C449 jet, the length unit of the simulation corresponds to $1'$.

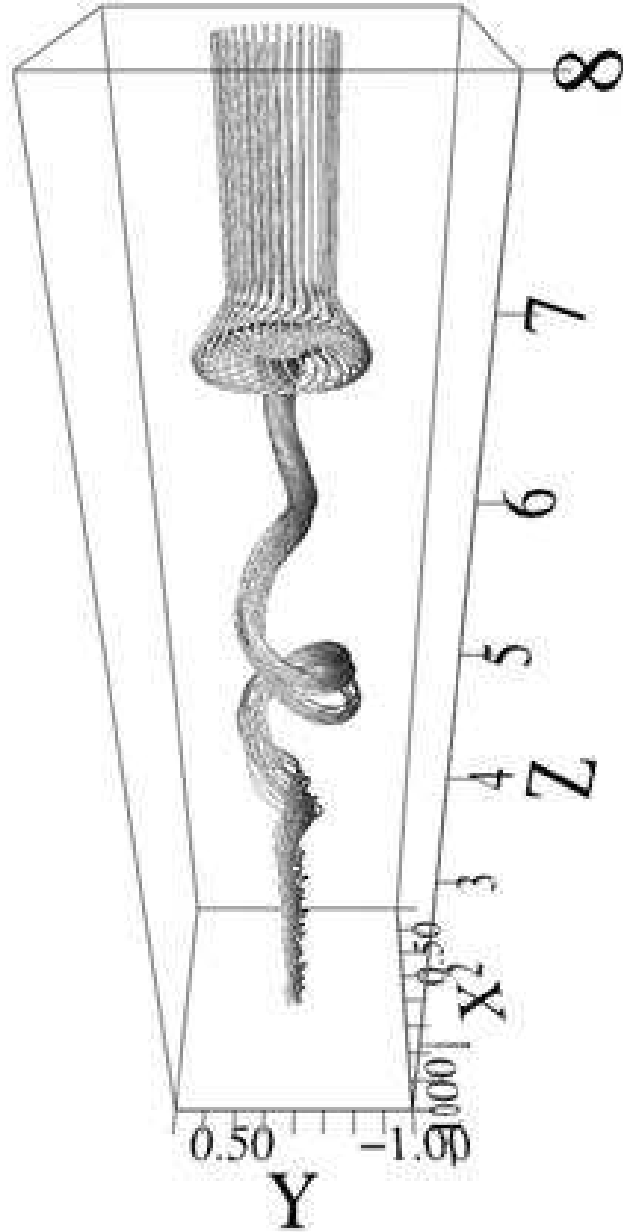


Fig. 17.— The 3-dimensional configuration of the selected magnetic lines of force seen at the best-fitting viewing angle at $t = 20.0$.

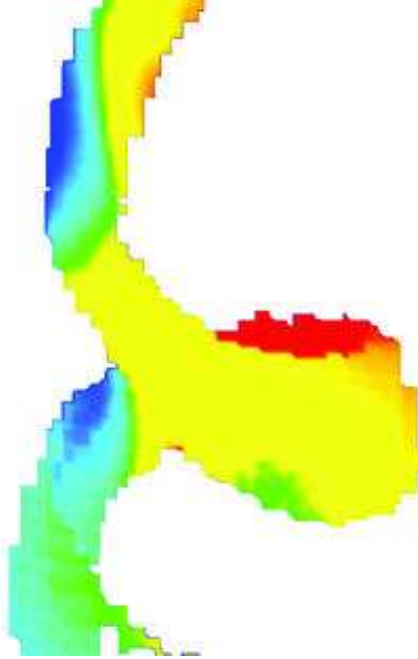


Fig. 18.— The distribution of Faraday rotation measure calculated by the integration of $n_e B_{\parallel}$.